NUMERICAL PREDICTION OF STAGNATION-POINT SHOCK-DETACHMENT DISTANCE FOR HYPERSONIC LOW-DENSITY FLOW OVER BLUNT NOSE SHAPES

Wilson F. N. Santos
Combustion and Propulsion Laboratory
National Institute for Space Research
Cachoeira Paulista, SP 12630-000 Brazil

Keywords: *Hypersonic flow, Rarefied Flow, DSMC, Blunt leading edge, Shock standoff distance*

Abstract

Computations using the Direct Simulation Monte Carlo method are presented for hypersonic flow over flat-nose leading edges. The primary aim of this paper is to examine the geometry effect of such leading edges on the shock wave structure. The sensitivity of shock wave shape, shock standoff distance, and shock thickness to shape variations of such leading edges is calculated by using a model that classifies the molecules in three distinct classes, i.e., "undisturbed freestream", "reflected from the boundary" and "scattered", i.e., molecules that had been indirectly affected by the presence of the leading edge. Comparisons are made between these new blunt configurations and circular cylinder shape based on shock wave standoff distance and shock wave thickness. It was found that the new blunt leading edges provided smaller shock wave standoff distance and shock wave thickness, compared to the corresponding circular cylinder.

1   Introduction

The successful design of high-lift, low-drag hypersonic configurations will depend on the ability to incorporate relatively sharp leading edges that combine good aerodynamic properties with acceptable heating rates. Certain configurations, such as hypersonic waveriders [1], are designed analytically with infinitely sharp leading edge for shock wave attachment. However, for practical applications, these sharp leading edges must be blunted for heat transfer, manufacturing, and handling concerns, with associated departures from ideal performance. Typically, a round leading edge (circular cylinder) with constant radius of curvature near the stagnation point has been chosen. Nevertheless, shock detachment distance on a cylinder, with associated leakage, scales with the radius of curvature. Certain classes of non-circular shapes may provide the required bluntness with smaller shock separation than round leading edges, thus allowing manufacturing, and ultimately heating control, with reduced aerodynamic losses.

A typical blunt body, composed of a flat nose followed by a highly curved, but for the most part slightly inclined afterbody surface, may provide the required bluntness for heat transfer, manufacturing and handling concerns with reduced departures from ideal aerodynamic performance. This conception is based on work of Reller [2], who has pointed out that this shape results from a method of designing low heat transfer bodies. According to Reller [2], low heat transfer bodies is devised on the premise that the rate of heat transfer to the nose will be low if the local velocity is low, while the rate of heat transfer to the afterbody will be low if the local density is low.

Santos [3] has investigated the effect of the leading edge thickness on the aerodynamic sur-

face quantities over these flat-nose leading edges. The thickness effect was examined for a range of Knudsen number, based on the thickness of the flat nose, covering from the transitional flow regime to the free molecular flow regime. The emphasis of the work was to compare the heat transfer and drag of this new shape with those obtained for round leading edge. It was found that flat-nose leading edges provided lower drag than round leading edge. Nevertheless, round leading edge gave smaller stagnation point heating than the flat nose leading edges for the conditions investigated.

Based on recent interest in hypersonic waveriders for high-altitude/low-density applications [4, 5, 6, 7], this paper extends the analysis presented by Santos [3] by investigating computationally the shock wave structure over these new contours. The primary goal is to assess the sensitivity of the shock standoff distance, shock wave thickness and shock wave shape to variations in the thickness of the leading edge and to compare them to the round leading edges shape (circular cylinder). Comparisons based on shock standoff distance are made to examine the benefits and disadvantages of using these new blunt shapes over round shapes.

For the transitional hypersonic flow, at high Mach number and high altitude, the flow departs from thermal equilibrium and the energy exchange into the various modes due to the vibrational excitation and relaxation becomes important. For the high altitude/high Knudsen number of interest ($Kn > 0.1$), the flowfield is sufficiently rarefied that continuum method is inappropriate. Alternatively, the DSMC method is used in the current study to calculate the rarefied hypersonic two-dimensional flow on the leading edge shapes.

2   Body Shape Definition

In dimensionless form, the contour that defines the shape of the afterbody surface is given by the following expression,

$$\overline{x} \;=\; \int_{1}^{\overline{y}_{max}} \sqrt{\overline{y}^{k} - 1}\, d\overline{y} \qquad (1)$$
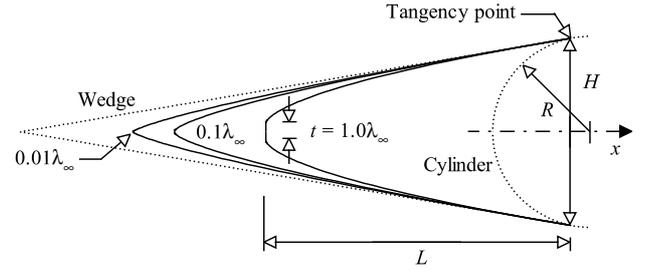

Fig. 1 Drawing illustrating the leading edge geometries.

where $\overline{x} = x/y_{nose}$ and $\overline{y} = y/y_{nose}$.

The flat-nose leading edges are modeled by assuming a sharp leading edge of half angle θ with a circular cylinder of radius R inscribed tangent to this wedge. The flat-nose leading edges, inscribed between the wedge and the cylinder, are also tangent to them at the same common point where they have the same slope angle. It was assumed a leading edge half angle of 10 deg, a circular cylinder diameter of 10^{-2}m and flat-nose thicknesses t/λ_{∞} of 0.01, 0.1 and 1, where $t = 2y_{nose}$ and λ_{∞} is the molecular freestream mean free path. Figure 1 illustrates this construction for the set of shapes investigated. From geometric considerations, the exponent k in Eq.(1) is obtained by matching slope on the wedge, on the circular cylinder and on the body shapes at the tangency point. For dimensionless thicknesses of 0.01, 0.1 and 1, the exponent k corresponds to 0.501, 0.746 and 1.465, respectively. The common body height H and the body length L are obtained in a straightforward manner.

3   Computational Method

The Direct Simulation Monte Carlo (DSMC) method, pioneered by Bird [8], has become one of the standard and reliable successful numerical techniques for modeling complex flows in the transition regime. The transition regime is the category of flow that falls between the continuum regime, where the Navier-Stokes equations are valid, and the free molecular regime, which is the limit of infinite Knudsen number.

In the DSMC method, a group of represen-

tative molecules are tracked as they move, collide and undergo boundary interactions in simulated physical space. Each simulated molecule represents a very much larger number of real molecules. The molecular motion, which is considered to be deterministic, and the intermolecular collisions, which are considered to be stochastic, are uncoupled over the small time step used to advance the simulation and computed sequentially. The simulation is always calculated as unsteady flow. However, a steady flow solution is obtained as the large time state of the simulation.

The molecular collisions are modeled using the variable hard sphere(VHS) molecular model [9]. The energy exchange between kinetic and internal modes is controlled by the Borgnakke-Larsen statistical model [10]. Simulations are performed using a non-reacting gas model consisting of two chemical species, N_2 and O_2. Energy exchanges between the translational and internal modes are considered. For this study, the relaxation numbers of 5 and 50 were used for the rotation and vibration, respectively.

The flowfield is divided into a number of regions, which are subdivided into computational cells. The cells are further subdivided into four subcells, two subcells/cell in each coordinate direction. The cell provides a convenient reference for the sampling of the macroscopic gas properties, while the collision partners are selected from the same subcell for the establishment of the collision rate. The linear dimensions of the cells should be small in comparison with the scale length of the macroscopic flow gradients normal to the streamwise directions, which means that the cell dimensions should be of the order of the local mean free path or even smaller [8].

The computational domain used for the calculation is made large enough so that body disturbances do not reach the upstream and side boundaries, where freestream conditions are specified. A schematic view of the computational domain is depicted in Fig. 2. Side I is defined by the body surface. Diffuse reflection with complete thermal accommodation is the condition applied to this side. Advantage of the flow symmetry is taken into account, and molecular simulation is
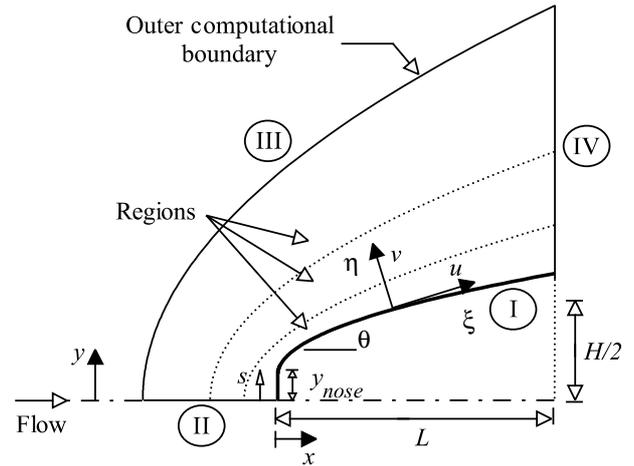

Fig. 2 Schematic view of the computational domain.

applied to one-half of a full configuration. Thus, side II is a plane of symmetry, where all flow gradients normal to the plane are zero. At the molecular level, this plane is equivalent to a specular reflecting boundary. Side III is the freestream side through which simulated molecules enter and exit. Finally, the flow at the downstream outflow boundary, side IV, is predominantly supersonic and vacuum condition is specified [8]. At this boundary, simulated molecules can only exit.

Numerical accuracy in DSMC method depends on the grid resolution chosen as well as the number of particles per computational cell. Both effects were investigated to determine the number of cells and the number of particles required to achieve grid independence solutions. Grid independence was tested by running the calculations with half and double the number of cells in ξ and η directions (see Fig. 2) compared to a standard grid. Solutions (not shown) were near identical for all grids used and were considered fully grid independent.

4 Flow Conditions

The freestream conditions and the gas properties used in the present calculations are those given by Santos [3] and summarized in Table 1.
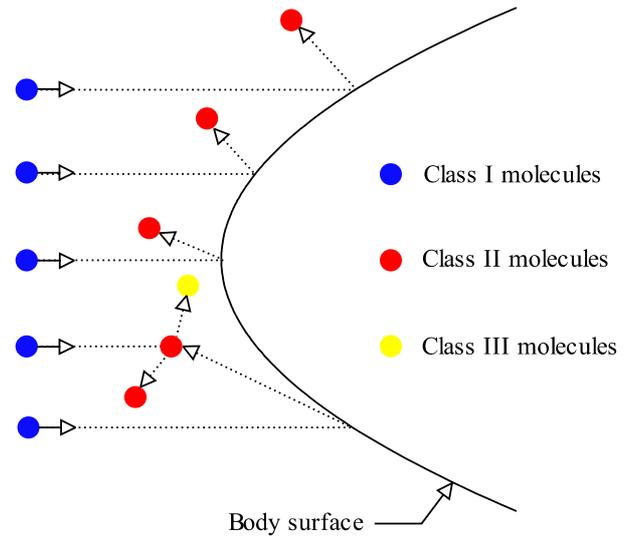
The freestream velocity V_∞ is assumed to

3

Table 1 Freestream conditions and gas properties

Parameter	Value	Unit
Temperature (T_∞)	220.0	K
Pressure (p_∞)	5.582	N/m^2
Density (ρ_∞)	8.753×10^{-5}	kg/m^3
Viscosity (μ_∞)	1.455×10^{-5}	Ns/m^2
Number density (n_∞)	1.8209×10^{21}	m^{-3}
Mean free path (λ_∞)	9.03×10^{-4}	m
Molecular mass O_2	5.312×10^{-26}	kg
Molecular mass N_2	4.650×10^{-26}	kg
Molecular diameter O_2	4.01×10^{-10}	m
Molecular diameter N_2	4.11×10^{-10}	m
Mole fraction O_2	0.237	
Mole fraction N_2	0.763	
Viscosity index O_2	0.77	
Viscosity index N_2	0.74	

Fig. 3 Drawing illustrating the classification of molecules.

be constant at 3.56 km/s, which corresponds to freestream Mach number M_∞ of 12. The wall temperature T_w is assumed constant at 880 K. The overall Knudsen number Kn_t, defined as the ratio of the freestream mean free path λ_∞ to the leading edge thickness t, corresponds to 100, 10 and 1 for flat-nose thicknesses t/λ_∞ of 0.01, 0.1 and 1, respectively. The Reynolds number Re_t covers the range from 0.193 to 19.3, based on conditions in the undisturbed stream with leading edge thickness t as the characteristic length.

5 Computational Procedure

The problem of predicting the shape and location of detached shock waves has been stimulated by the necessity for blunt noses and leading edges configurations designed for hypersonic flight in order to cope with the aerodynamic heating. Also, the ability to predict the shape and location of shock waves is of primary importance in analysis of aerodynamic interference. In addition, displacement of the shock wave is especially undesirable in a waverider geometry [1], because these hypersonic configurations usually depend on shock wave attachment at the leading edge to achieve their high lift-to-drag ratio at high-lift co-

efficient.

In order to study the shock wave structure, the shape, the thickness and the detachment of the shock wave are quantified by employing the following procedure: the flow is assumed to consist of three distinct classes of molecules; those molecules from the freestream that have not been affected by the presence of the leading edge are denoted as class I molecules; those molecules that, at some time in their past history, have struck and been reflected from the body surface are denoted as class II molecules; and those molecules that have been indirectly affected by the presence of the body are defined as class III molecules. Figure 3 illustrates the classification of the molecules.

It is assumed that the class I molecule changes to class III molecule when it collides with class II or class III molecule. Class I or class III molecule is progressively transformed into class II molecule when it interacts with the body surface. Also, a class II molecule remains class II regardless of subsequent collisions and interactions. Hence, the transition from class I molecules to class III molecules may represent the shock wave, and the transition from class III to class II may define the boundary layer.
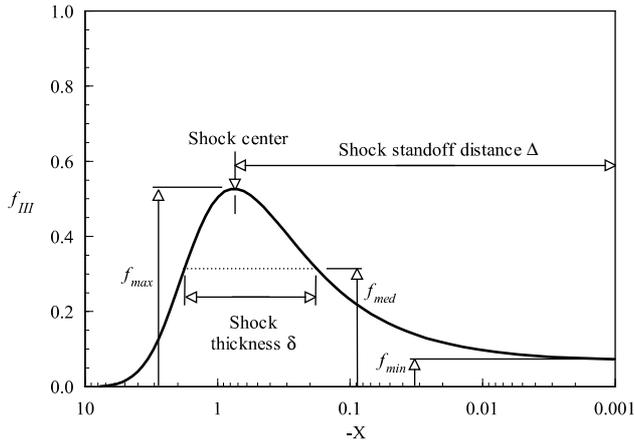
Fig. 4 Schematic of shock wave structure.

A typical distribution of class III molecules along the stagnation streamline for blunt leading edges is displayed in Fig. 4 along with the definition used to determine the thickness, displacement and shape of the shock wave. In this figure, X is the distance x along the stagnation streamline (see Fig. 2), normalized by the freestream mean free path λ_∞.

In a rarefied flow, the shock wave has a finite region that depends on the transport properties of the gas, and can no longer be considered as a discontinuity obeying the classical Rankine-Hugoniot relations. In this context, the shock standoff distance Δ is defined as being the distance between the shock wave center and the nose of the leading edge along the stagnation streamline. As shown in Fig. 4, the center of the shock wave is defined by the station that corresponds to the maximum value for f_{III}. The shock wave thickness δ is defined by the distance between the stations that correspond to the mean value for f_{III}. Finally, the shock wave shape (shock wave "location") is determined by the coordinate points given by the maximum value in the f_{III} distribution along the lines departing from the body surface, i.e., η-direction as shown in Fig. 2.

The molecule classification that has been adopted here was first presented by Lubonski [11] in order to study the hypervelocity Couette flow near the free molecule regime. Lubonski [11] divided the gas into three classes of molecules: "freestream", "reflected from the boundary" and "scattered". Later, for the purpose of flow visualization, Bird [12] applied the same scheme of classification by identifying the classes by colors: blue for class I, red for class II and yellow for class III molecules.

6 Computational Results and Discussion

The purpose of this section is to discuss and to compare differences in the shape, thickness and displacement of the shock wave due to variations in the leading edge thickness and to compare them to those obtained for the cylinder shape that generated the blunt shapes.

The distribution of molecules for each class along the stagnation streamline is demonstrated in Fig. 5 for cases t/λ_∞ of 0.01, 0.1 and 1. In this figure, f_I, f_{II} and f_{III} are the ratio of the number of molecules for class I, II and III, respectively, to the total amount of molecules inside each cell. For comparison purpose, the distribution of molecules for the circular cylinder is illustrated in Fig. 6.

6.1 Shock Wave Standoff Distance

According to the definition shown in Fig. 4, the shock wave standoff distance Δ can be observed in Fig. 5 for the flat-nose shapes and in Fig. 6 for the circular cylinder. It is apparent from this set of figures that there is a discrete shock standoff distance for all cases investigated. The calculated shock wave standoff distance Δ, normalized by the freestream mean free path λ_∞, is 0.201, 0.346 and 0.753 for t/λ_∞ of 0.01, 0.1 and 1, respectively. Compared to flat-nose shapes, the circular cylinder provides a larger shock detachment, i.e., Δ/λ_∞ of 1.645. This value is about 8.2, 4.8 and 2.2 times larger than the cases corresponding to t/λ_∞ of 0.01, 0.1 and 1, respectively. The results tend to confirm the expectation that the shock standoff distance for sharp leading edge is smaller than that for blunt leading edge, i.e., it decreases with decreasing the thickness of the leading edge for the cases investigated.

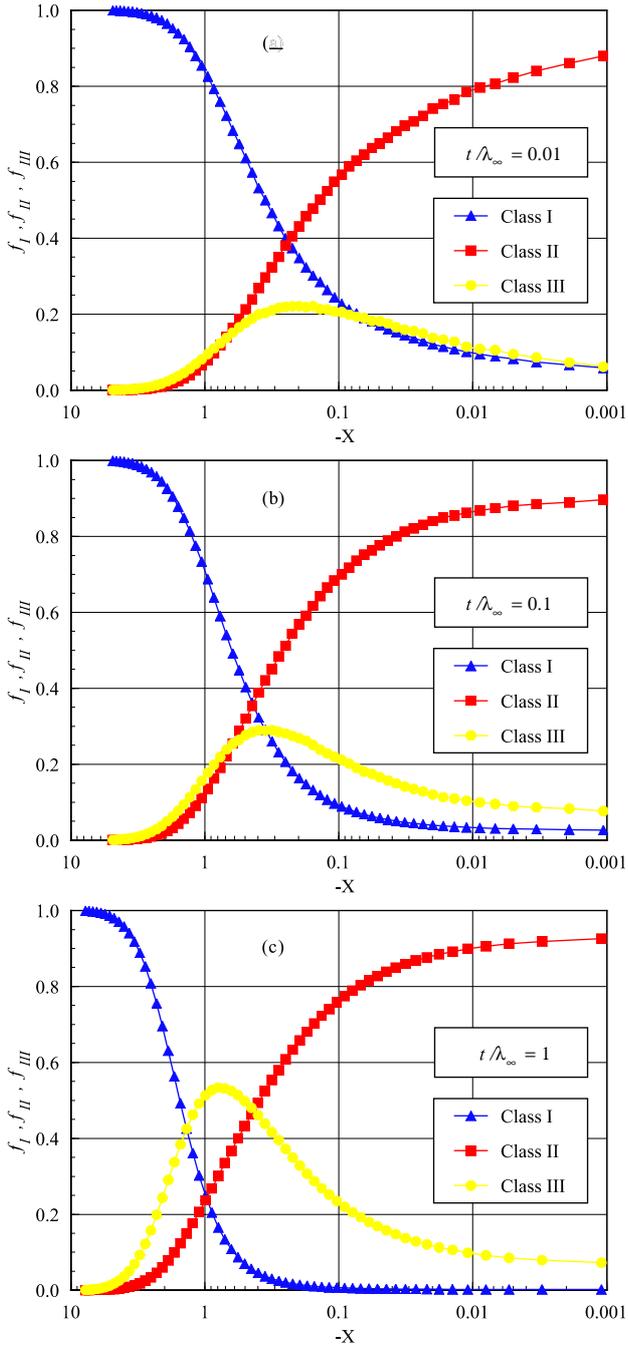It is worth mentioning that shock standoff

Fig. 6 Distributions of molecules for classes I, II and III along the stagnation streamline for the circular cylinder.

propriate than the circular cylinder, since they present reduced shock wave detachment distances. Nevertheless, smaller shock detachment distance is associated with a higher heat load to the nose of the body (Santos [3]).

6.2 Shock Wave Thickness

According to the definition of the shock wave thickness shown in Fig. 4, the shock wave thickness δ along the stagnation streamline can be obtained in Fig. 5 for the flat-nose shapes and in Fig. 6 for the circular cylinder. The shock wave thickness δ, normalized by the freestream mean free path λ_∞, is 0.652, 0.863 and 1.673 for t/λ_∞ of 0.01, 0.1 and 1, respectively. The circular cylinder provides a larger shock thickness, i.e., δ/λ_∞ of 3.350. Compared to the flat-nose shapes, this value is about 5.3, 3.9 and 2.0 times larger than the cases corresponding to t/λ_∞ of 0.01, 0.1 and 1, respectively.

6.3 Shock Wave Shape

The shock wave shape, defined by the shock wave center, is obtained by calculating the position that corresponds to the maximum f for class III molecules in the η-direction along the body surface (see Fig. 2). Figure 7 illustrates the shock wave shape in the vicinity of the stagnation

distance becomes important in hypersonic vehicles such as waveriders, which depend on leading edge shock attachment to achieve their high lift-to-drag ratio at high lift coefficient. In this context, the flat-nose shapes seem to be more ap-
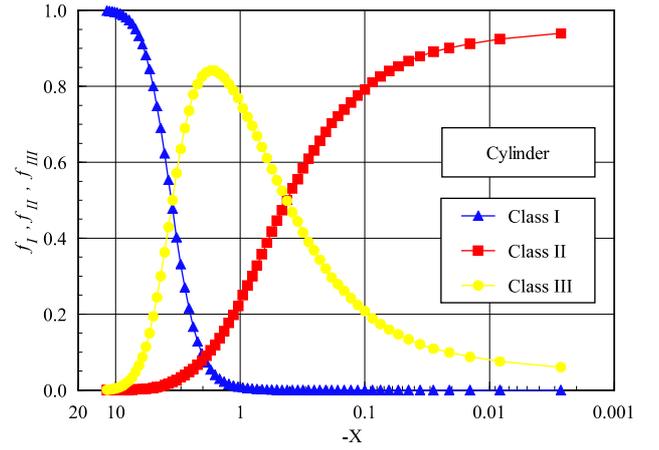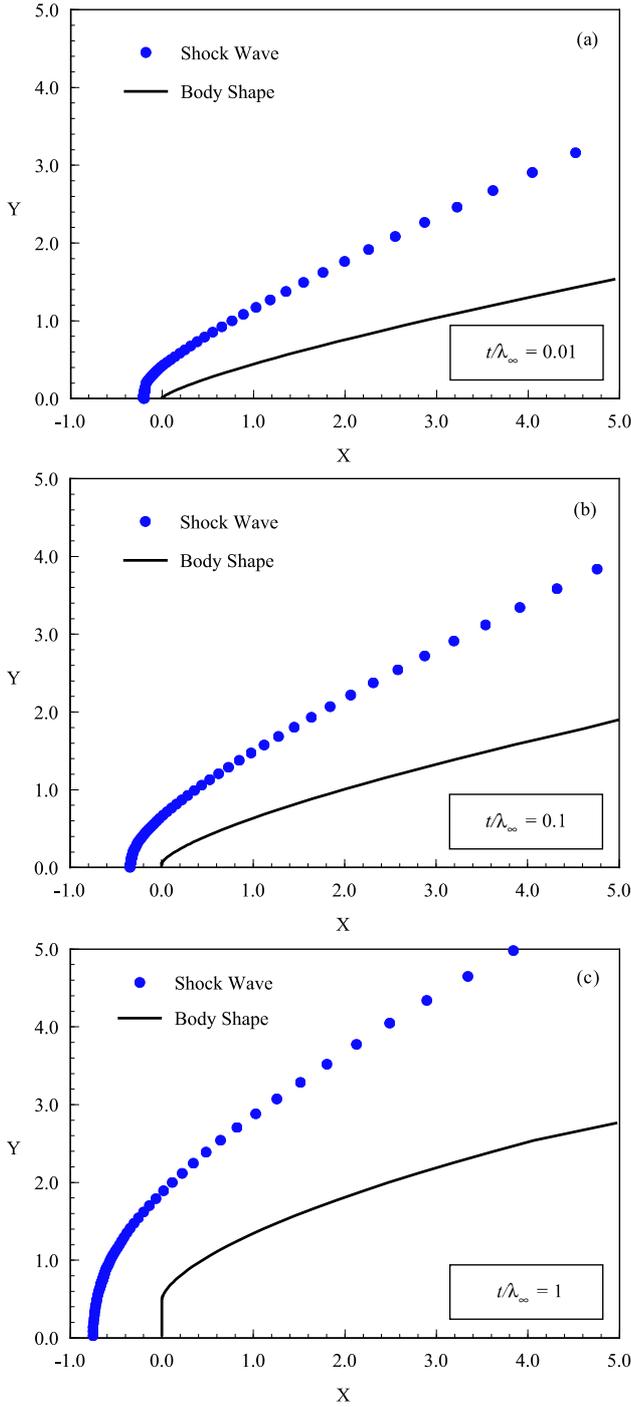
Fig. 7 Shock wave shapes on flat-nose bodies with thickness t/λ_∞ of (a) 0.01, (b) 0.1 and (c) 1.

region for the flat-nose bodies with thicknesses t/λ_∞ of 0.01, 0.1 and 1, respectively. In this set of plots, X and Y are the cartesian coordinates x and y normalized by λ_∞.

It was pointed out by Lees and Kub-ota [13] that when the freestream Mach number M_∞ is sufficiently large, the hypersonic small-disturbance equations admit similarity solutions for the asymptotic shock wave shapes over power-law bodies ($y \propto x^n, 0 < n < 1$), where asymptotic refers to the flowfield at large distances downstream of the nose of the body. The hypersonic small-disturbance theory states that, for certain exponent n, a body defined by x^n produces a shock wave of similar shape and profiles of flow properties transverse to the stream direction that are similar at any axial station not too near the nose. At or near the nose, the surface slope, the curvature, and the higher derivatives are infinite, and the similarity solutions break down. In the more general case for $0 < n < 1$, the shock wave grows as x^m. When n grows from zero, m begins by keeping the constant value $m = 2/(j+3)$, and if n keeps on growing towards unity, m remains equal to n. Here j takes the values zero for planar flow and one for axisymmetric flow.

The flat-nose bodies investigated in this work are not power-law shapes themselves, by they can be closely fitted with power-law shapes ($\propto x^n$). Figure 8(a) depicts the comparison of the flat-nose shapes and the power-law curve fit shapes. As would be expected, discrepancies have been found among the curves in the vicinity of the nose of the bodies. This behavior is brought out more clearly in Fig. 8(b), which exhibits details of the curves near the nose.

By considering the reference system located at the nose of the flat-nose bodies, $X = 0$, the fitting process, which has been performed over those bodies shown in Fig. 8, approximates the body shapes by power-law shape of the following form,

$$y = a(x+b)^n \qquad (2)$$

where a is the power-law constant of the curve fit, b is the distance from the nose of the leading edge, and n is the power law exponent of the curve fit. The coefficients a and b, normalized, respectively, by λ_∞^{1-n} and λ_∞, and the exponent n are tabulated in Table 2.
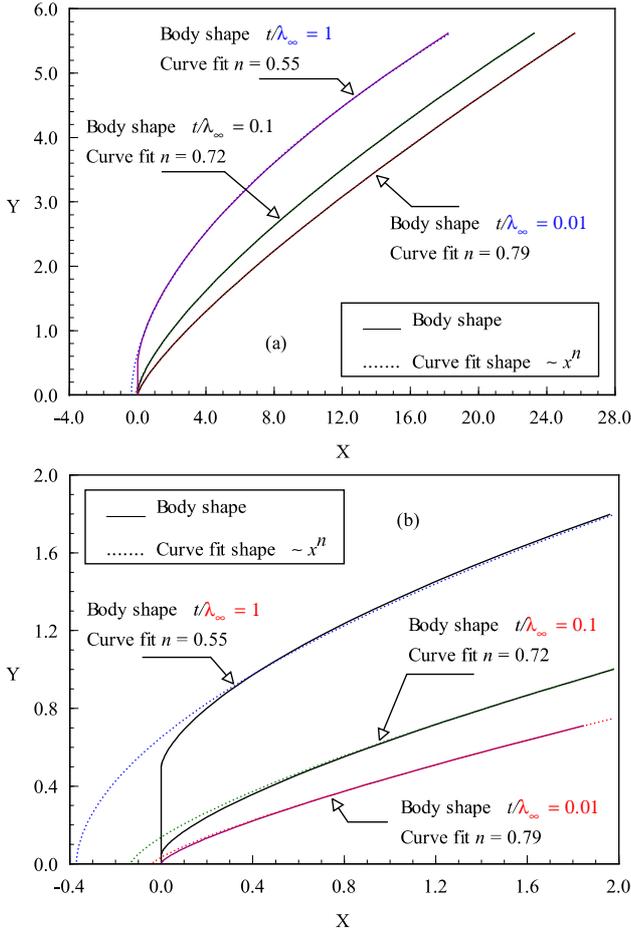
Fig. 8 Comparison of flat-nose shapes with power-law curve fit shapes for thickness t/λ_∞ of 0.01, 0.1 and 1, (a) along the total length L, and (b) in the vicinity of the nose.

By considering that the flat-nose leading edges are well represented by power-law leading edges far from the nose of the leading edges and by assuming that power-law bodies generate power-law shock waves in accordance with hypersonic small-disturbance theory (Lees and Kubota [13]), the shock location coordinates shown in Fig. 7 were used to approximate the shape of the shock wave with a curve fit. A fitting algorithm was performed over these points to approximate the shock shape as a power law curve of the following form,

$$y = A(x+B)^m \qquad (3)$$

where A is the shock wave power law constant, B

Table 2 Dimensionless coefficients a, b and n for the curve fit power-law bodies.

t/λ_∞	a	b	n
0.01	0.42893	0.04120	0.55
0.1	0.58436	0.13318	0.72
1	1.12387	0.37067	0.79

is the distance from the nose of the leading edge to the shock wave curve fit along the stagnation streamline, and m is the shock wave power law exponent.

In order to compare the shock wave shapes obtained in this work with those predicted by Lees and Kubota [13], two forms of the curve fit were considered in defining the shock shape: (1) A, B and m were found to provide the best curve fit solutions, and (2) A and B were found by keeping $m = 2/3$ for $n \leq 2/3$ cases, and $m = n$ for $n > 2/3$ cases, where n and m stand for body and shock wave power law exponents, respectively.

It is important to mention that the fitting process was performed over the points yielded by DSMC simulations located far from the nose region, say $X > 1.0$, where it is expected that the blunt nose effects are not significant. It is important to recall that the shock wave shape in the vicinity of the nose is not correctly predicted by the theoretical solutions, since the hypersonic slender body approximations are violated close to or at the nose of the leading edges as explained above. Moreover, the flat-nose shapes are represented by power-law shapes far from the nose region, as displayed in Fig. 8.

Curve fit solutions for shock shape over a flat-nose body with $t/\lambda_\infty = 0.01$, which corresponds to a body power law exponent of 0.79, are displayed in Fig. 9(a). In this figure, the solutions given by $m = 0.84$ and $m = n = 0.79$ represent, respectively, the two forms of the curve fit solutions mentioned above. It is apparent from this figure that both curve fits match the shock wave shape obtained by the DSMC simulation. This is

in qualitative agreement with the Lees and Kubota [13] findings in the sense that the shock wave shape would follow the shape of the body for body power law exponent $n > 2/3$.

Figure 9(b) illustrates the curve fit solutions for shock shape over a flat-nose body with $t/\lambda_\infty = 0.1$, which corresponds to a body power law exponent of 0.72. It is observed from this figure that both curve fits match the shock wave shape obtained by the DSMC simulation. Nevertheless, the curve fit shock wave given by $m = 0.80$ yields a better agreement, specially closer to the nose of the leading edge.

Shock shape curve fit solutions for the flat-nose body with $t/\lambda_\infty = 1$, which corresponds to a body power law exponent of 0.55, are displayed in Fig. 9(c). For this body shape, three curve fits were obtained; in the first case m was set equal to the body shape, $m = n = 0.55$; in the second case, the best fit was found for $m = 0.71$; in the third case, m was set equal to 2/3, the exponent that it is expected that the shock wave would grow, according to the theory (Lees and Kubota [13]). Referring to Fig. 9(c), it is noted that the curve fit given by $m = n = 0.55$ does not match the shock wave shape obtained by the DSMC simulation. In contrast, the two other curve fit solutions, m equal to 2/3 and 0.71 present an excellent agreement with that solution provided by the DSMC simulation. Once again, the curve-fitted solution deviates from the DSMC solution close

Table 3 Dimensionless coefficients *A*, *B* and *m* for the shock wave curve fit.

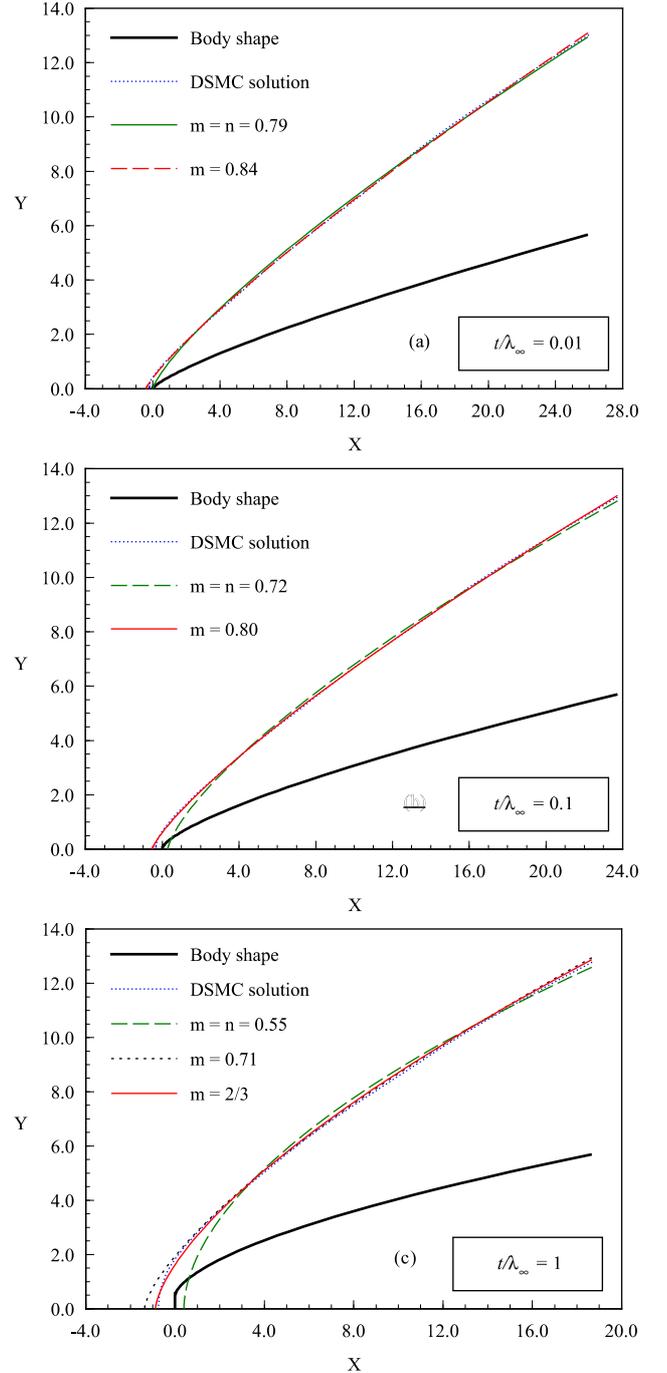| t/λ_∞	A	B	m
0.01	0.98885	3.10938×10^{-4}	0.79
0.01	0.83933	0.40477	0.84
0.1	1.32255	-0.28812	0.72
0.1	1.01519	0.53395	0.80
1	2.54848	-0.39788	0.55
1	1.55057	1.37132	0.71
1	1.77429	0.87559	0.667

Fig. 9 Shock wave shapes curve fits on flat-nose bodies with thickness t/λ_∞ of (a) 0.01, (b) 0.1 and (c) 1.

to the nose of the leading edge, as would be expected. For comparison purpose, the coefficients *A* and *B*, normalized, respectively, by λ_∞^{1-n} and λ_∞, and the exponent *m* are tabulated in Table 3.

7   Conclusions

This study applies the Direct Simulation Monte Carlo method to assess the impact on the shock wave structure due to variations in the shape of flat-nose leading edges. The calculations have provided information concerning the nature of the shock wave detachment distance, shock wave thickness and shock wave shape resulting from variations in the thickness of the flat nose for the idealized situation of two-dimensional hypersonic rarefied flow. The emphasis of the investigation was also to compare these flat-nose leading edges with round shape in order to determine which geometry is better suited as a blunting profiles in terms of the shock wave standoff distance.

It was found that the shock wave standoff distance and the shock wave thickness for the flat-nose bodies are lower than that for the circular body with the same tangency to a wedge of specified oblique angle. In addition, the computational results indicated that the shock wave shape grows with power law form ($\propto x^m$), in agreement with the hypersonic small disturbance theory, for the flat-nose bodies investigated, which can be closely fitted with power-law shapes ($\propto x^n$).

References

[1] Nonweiler, T. R. F.,"Aerodynamic problems of manned space vehicles," *J. of the Royal Aeronautical Society*, Vol. 63, Sept, 1959, pp.521-528.

[2] Reller Jr., J. O., "Heat transfer to blunt nose shapes with laminar boundary layers at high supersonic speeds", NACA RM-A57FO3a, 1957.

[3] Santos, W. F. N., "Aerodynamic heating on blunt nose shapes in rarefied hypersonic flow", in *17th International Congress of Mechanical Engineering COBEM 2003*, 10-14 November 2003, São Paulo, SP, Brazil.

[4] Anderson, J. L., "Tethered aerothermodynamic research for hypersonic waveriders", in *Proceedings of the 1st International Hypersonic Waverider Symposium*, Univ. of Maryland, College Park, MD, 1990.

[5] Potter, J. L. and Rockaway, J. K., "Aerodynamic optimization for hypersonic flight at very high altitudes", in *Rarefied gas Dynamics: Space Science and Engineering*, edited by B. D. Shizgal and D. P. Weaver, Vol. 160, Progress in Astronautics and Aeronautics, AIAA New York, 1994, pp.296-307.

[6] Rault, D. F. G., "Aerodynamic characteristics of a hypersonic viscous optimized waverider at high altitude", *J. of Spacecraft and Rockets*, Vol. 31, No. 5, 1994, pp.719-727.

[7] Graves, R. E. and Argrow, B. M., "Aerodynamic performance of an osculating-cones waverider at high altitudes", in *35th AIAA Thermophysics Conference*, AIAA Paper 2001-2960, Anaheim, CA, 2001.

[8] Bird, G. A.,*Molecular gas dynamics and the direct simulation of gas flows*, Oxford University Press, Oxford, England, UK, 1994.

[9] Bird, G. A., "Monte Carlo simulation in an engineering context", in *Progress in Astronautics and Aeronautics: Rarefied gas Dynamics*, edited by Sam S. Fisher, Vol. 74, part I, AIAA New York, 1981, pp.239-255.

[10] Borgnakke, C. and Larsen, P. S., "Statistical collision model for Monte Carlo simulation of polyatomic gas mixture", *Journal of computational Physics*, vol. 18, No. 4, 1975, pp.405-420.

[11] Lubonski, J., "Hypersonic plane couette flow in rarefied gas", in *Archiwum Mechaniki Stosowanej*, vol. 14, No. 3/4, 1962, pp.553-560.

[12] Bird, G. A., "The structure of rarefied gas flows past simple aerodynamic shapes", in *J. of Fluid Mechanics*, vol. 36, No. 3, 1969, pp.571-576.

[13] Lees, L. and Kubota, T., "Inviscid hypersonic flow over blunt-nosed slender bodies", *Journal of Aeronautical Sciences*, Vol. 24, No. (3), 1957, pp. 195–202.